Available online at www.sciencedirect.com
SCIENCE DIRECT®
Journal of Nuclear Materials 351 (2006) 261–268
journal of nuclear materials
www.elsevier.com/locate/jnucmat

Characterization of precipitates in MA/ODS ferritic alloys

M.K. Miller *, K.F. Russell, D.T. Hoelzer

Metals and Ceramics Division, Oak Ridge National Laboratory, P.O. Box 2008, Bldg 4500S, MS 6136, Oak Ridge, TN 37831-6136, USA

Abstract

Mechanically alloyed, oxide dispersion strengthened (MA/ODS) ferritic alloys are attractive for fusion reactor applications because of their potential for operation at high temperatures and also because the dispersed oxide particles may provide a trap for transmutant helium. The microstructural stability of MA/ODS Fe–14 wt% Cr–3% W–0.4% Ti–0.3% Y_2O_3 ferritic alloys was investigated by atom probe tomography. Atom probe tomography revealed that these MA/ODS 14YWT ferritic alloys contain a high number density of nanometer scale titanium-, yttrium- and oxygen-enriched nanoclusters in the as-extruded condition. These nanoclusters were found to be extremely resistant to coarsening at temperatures of at least 1000 °C.
Published by Elsevier B.V.

1. Introduction

Neutrons (14 MeV) stemming from the plasma strike the first wall of the fusion reactor blanket produce damage in the form of atomic displacements of up to 200 dpa, the production of point defects, such as vacancies, both individual and clusters of vacancies, and self-interstitial atom (SIA) defects as well as transmutant helium with levels of up to 2000 appm. Therefore, alloys subjected to these high neutron fluences and temperatures of up to at least 500 °C can exhibit void swelling, dislocation evolution, phase and structural instabilities and grain boundary embrittlement by helium bubbles. In principle, these effects may be controlled through the use of alloys that contain high number densities of high sink strength nanometer-scale features to trap (getter) both the helium in fine bubbles and the radiation-induced defects to promote self-healing. Several steels have been considered for this first wall application, including the reduced activation ferritic/martensitic (RAF/M) Fe–7.5 wt% Cr–2% W F82H alloy. Recently, significant improvements in creep strength and high temperature stability were achieved in a mechanically alloyed oxide-dispersion-strengthened (MA/ODS) Fe–12.3 wt% Cr–3% W–0.4% Ti, −0.25% Y_2O_3 ferritic alloy designated 12YWT compared to the RAF/M F82H alloy [1–13]. These results suggest that further improvements in the high-temperature mechanical properties of iron base alloys may be achieved by producing a high-density of nano-particles in advanced nano-structured ferritic (NSF) alloys.

In this atom probe tomography [14] study, the stabilities of the fine scale particles in the microstructure of mechanically alloyed, oxide-dispersion-strengthened Fe–14 wt% Cr–3% W–0.4% Ti ferritic

* Corresponding author. Tel.: +1 865 574 4719; fax: +1 865 241 3650.
E-mail address: millermk@ornl.gov (M.K. Miller).

0022-3115/$ - see front matter Published by Elsevier B.V.
doi:10.1016/j.jnucmat.2006.02.004

alloys have been characterized after high temperature annealing at temperatures of up to 1000 °C (~0.65 T_m). Previous atom probe tomography characterizations of a MA/ODS 12YWT alloy with a nominal composition of Fe–12.3 wt% Cr–3% W–0.39% Ti–0.25% Y_2O_3 revealed the presence of high number densities of 2–4 nm diameter titanium-, yttrium- and oxygen-enriched nanoclusters in both the as-processed and crept conditions [7–12]. These nanoclusters were also detected in the ferrite after high temperature creep for up to 14 500 h at 800 °C, indicating a remarkable stability to coarsening. Similar nanoclusters have also been observed in the microstructures of three MA/ODS ferritic alloys (12YWT, 14YWT and a commercial tungsten-free, molybdenum-containing MA957 alloy) [13]. These nanoclusters have been characterized in the as-received condition and after isothermal heat treatments at temperatures up to 1300 °C (~85% T_m) [13].

Table 2
Compositions of the alloys used in this investigation. The balance is iron

Element	Alloy composition (at.%)		
	14YWT-CR	14YWT-SM	14WT-SM[a]
Cr	15.13	15.22	15.21
W	0.86	0.59	0.59
Ti	0.27	0.26	0.26
Si	0.30	0.06	0.06
Mn	0.64	0.17	0.17
Ni	0.22	0.21	0.21
Mo	0.006	0.006	0.006
Cu	0.018	0.009	0.009
V	0.011	0.011	0.011
Nb	0.006	0.006	0.006
S	0.009	0.007	0.007
O	0.31	0.35	0.23
N	0.44	0.56	0.56
C	0.16	0.17	0.17
Y	0.08	0.08	–

[a] Calculated from 14YWT-SM without Y_2O_3.

2. Material and sample preparation

The Fe–14 wt% Cr–3% W–0.4% Ti alloys investigated in this study were prepared from argon gas atomized pre-alloyed powders which were made by Special Metals, Inc. (SM) or Crucible Research (CR). Four alloys were prepared from these powders. Three samples of these alloys designated 14YWT were ball milled with 0.3 wt% Y_2O_3 powders (Nanophase, Inc.) with a particle size ranging from 17–31 nm. One sample designated 14WT was also ball milled without the Y_2O_3 powder. Therefore in addition to the absence of yttrium in the alloy, this alloy also had a lower oxygen content. The mixed powders were ball milled in a Zoz Simolayer CM high energy mill in an argon gas atmosphere and with a ball-to-powder mass ratio of 10:1. The information about the samples, the pre-alloyed powder manufacturer, the amount of Y_2O_3 powder that was mixed with the pre-alloyed powders, the initial particle size range of the powders, and the duration of ball milling process is summarized in Table 1. The compositions of these alloys are listed in Table 2.

After ball milling, the powder was transferred to a 50 mm diameter mild steel can, degassed in a vacuum of $\sim 10^{-2}$ mbar at 400 °C, and sealed. The powders were consolidated by heating the sealed cans for 1 h at 850 °C followed by extruding at 850 °C. Samples were cut from the extruded alloys. Some samples were also heat treated for 1 h at 1000 °C in a vacuum of $\sim 10^{-6}$ mbar.

3. Microstructural characterization

The microstructures of these alloys were characterized with the Oak Ridge National Laboratory local electrode atom probe. A specimen temperature of 60 K, a pulse repetition rate of 200 kHz and a pulse fraction of 20% were used for the analyses. Compared to previous types of atom probes, this new instrument has a significantly faster rate of data

Table 1
Summary of the alloy parameters and processing conditions

Sample number	Alloy designation	Metal particle size (μm)	Y_2O_3 content (wt%)	Y_2O_3 particle size (nm)	Milling time (h)
1	14WT-SM[a]	45–150	–	17–31	40
2	14YWT-SM[a]	45–150	0.3	17–31	40
3	14YWT-SM[a]	45–150	0.3	17–31	80
4	14YWT-CR[b]	<45	0.3	17–31	40

[a] Special metals.
[b] Crucible research.

acquisition and a larger field of view and hence a larger volume of analysis.

The presence of solute-enriched precipitates was determined with the maximum separation method [14,15]. This method is based on the premise that the distance between solute atoms in a solute-enriched precipitate is significantly smaller than that in the surrounding matrix. Therefore, the atoms that belong to a solute-enriched precipitate may be distinguished from those in the matrix based on a maximum separation distance, d_{max}. Computer simulations of random solid solutions with a body centered cubic α-Fe crystal ($a_0 = 0.288$ nm) and a detection efficiency of 60% were used to define the value of $d_{max} = 0.6$ nm and the minimum number of solute atoms associated with each cluster, $n_{min} = 25$, to exclude fluctuations consistent with the random solid solution. The size of the solute-enriched features was estimated in terms of the radius of gyration, which was determined from positions of the solute atoms in each cluster. The composition of each cluster was estimated with the envelope method with a grid spacing of 0.1 nm [14]. The number densities were estimated from the number of particles in the volume of analysis, where the volume was estimated from the number of atoms in the volume, the detection efficiency of the mass spectrometer and the atomic density of body centered cubic iron.

4. Results and discussion

The Vickers hardnesses of the 14WT and 14WYT alloys in the as-extruded condition and after thermal annealing for 1 h at 1000 °C are compared to the previously characterized as-processed 12YWT alloy in Table 3. The hardnesses of the as-extruded 14YWT alloys were slightly higher than the as-processed 12YWT. The hardnesses of the yttria-containing 14YWT alloy were ~40% higher than that of the yttria-free 14WT alloy. Some softening of all the alloys was observed after the 1 h at 1000 °C heat treatment.

The general microstructures of the 14WT and 14YWT-CR alloy in the as-extruded condition and after thermal annealing for 1 h at 1000 °C are shown in Fig. 1. Transmission electron microscopy revealed uniformly distributed grains and a non-uniform dispersion of titanium oxides with sizes ranging from ~10–50 nm in the 14WT alloy. Only a few such coarse particles were observed in the 14YWT alloy. The grains in both alloys were slightly elongated parallel to the extrusion direction. After extrusion, the grain size was ~1–2 μm in the 14WT alloy and ~0.2–0.5 μm in the 14YWT alloy. Annealing for 1 h at 1000 °C did not have a significant effect on the grain size or coarse precipitate size.

Titanium, oxygen, tungsten and chromium atom maps of the yttria-free 14WT alloy after extrusion are shown in Fig. 2. A low number density of diffuse titanium- and oxygen-enriched nanoclusters is evident. The number density of these ~4 nm diameter nanoclusters was estimated to be approximately 6×10^{22} m^{-3}. Similar nanoclusters were present after the thermal annealing treatment of 1 h at 1000 °C, as shown in Fig. 3. However, their number density had decreased to $\approx 1 \times 10^{22}$ m^{-3} and their size had increased to ≈10 nm, indicating that some coarsening had occurred during the annealing treatment. Some carbon was found to be associated with these nanoclusters.

Significantly higher number densities of ultrafine titanium-, oxygen- and yttrium-enriched nanoclusters were observed in both the as-extruded and thermally aged yttria-containing 14YWT materials, as shown in Figs. 4 and 5, respectively. The distribution of these nanoclusters was not uniform with some layering of the nanoclusters evident. Two of these layers are viewed edge-on in Fig. 4(a). The distribution of these nanoclusters was also not uniform

Table 3
Vicker hardnesses (VPN) of the 14WT and 14YWT alloys in the as-extruded condition and after 1 h at 1000 °C. Data from the 12YWT in the as-processed condition and after 1 h at 1300 °C are included for comparison

Condition	12YWT		14WT-SM 40 h mill		14YWT-SM 40 h mill		14YWT-SM 80 h mill		14YWT-CR 40 h mill	
	Hardness	SD	Hardness	SD	Hardness	SD	Hardness	SD	Hardness	SD
As-processed	411.2	16.1								
As-extruded			325.4	13.8	459	4.6	465.3	13.7	451.2	12
1000 °C/1 h			254.8	9.3	377	6.1	440.9	12.9	386	33.6
1300 °C/1 h	298.5	6.2								

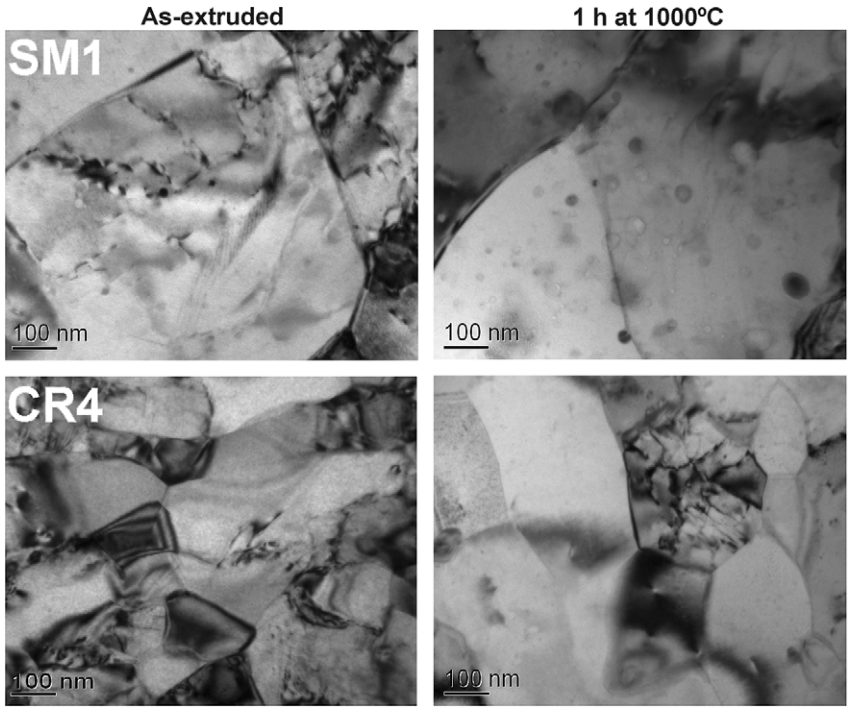

Fig. 1. Transmission electron micrographs of the 14WT-SM1 and 14YWT-CR4 alloys after extrusion and thermal annealing for 1 h at 1000 C.

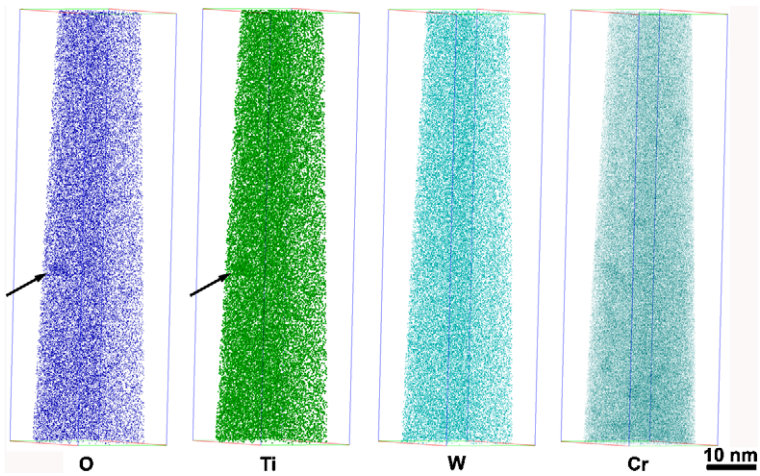

Fig. 2. Atom maps of the 14WT-SM1 alloy after extrusion. One titanium- and oxygen-enriched particle is evident in this volume.

within the two-dimensional layers. This non-uniform distribution of nanoclusters yielded a range in the number density from approximately $1–7 \times 10^{23}$ m^{-3}. The chromium was also enriched in these layers possibly from the incorporation of some chromium oxide from the surface of the powder. This local variation may be due to the residual effect of surface oxidation of the powder and the mechanical milling process leaving a non-uniform oxygen distribution, and suggests that the homogenization of the alloy during milling was incomplete. Alternatively, these layers of nanoclusters may be forming preferentially on grain boundaries due to enhanced nucleation at and diffusion along the boundary. This range of number densities is higher than that observed in the yttria-free 14WT alloy. The higher

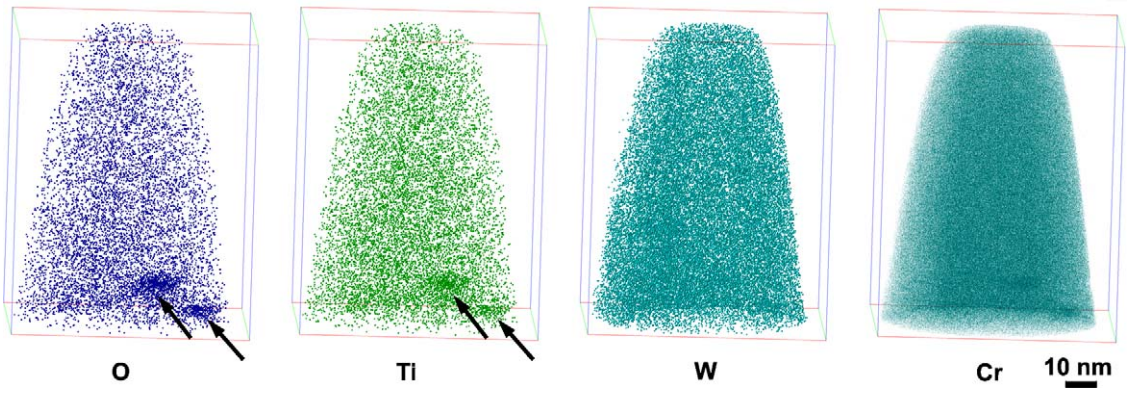

Fig. 3. Atom maps of the 14WT-SM1 alloy after thermal annealing for 1 h at 1000° C. Two titanium- and oxygen-enriched nanoclusters are evident in this volume.

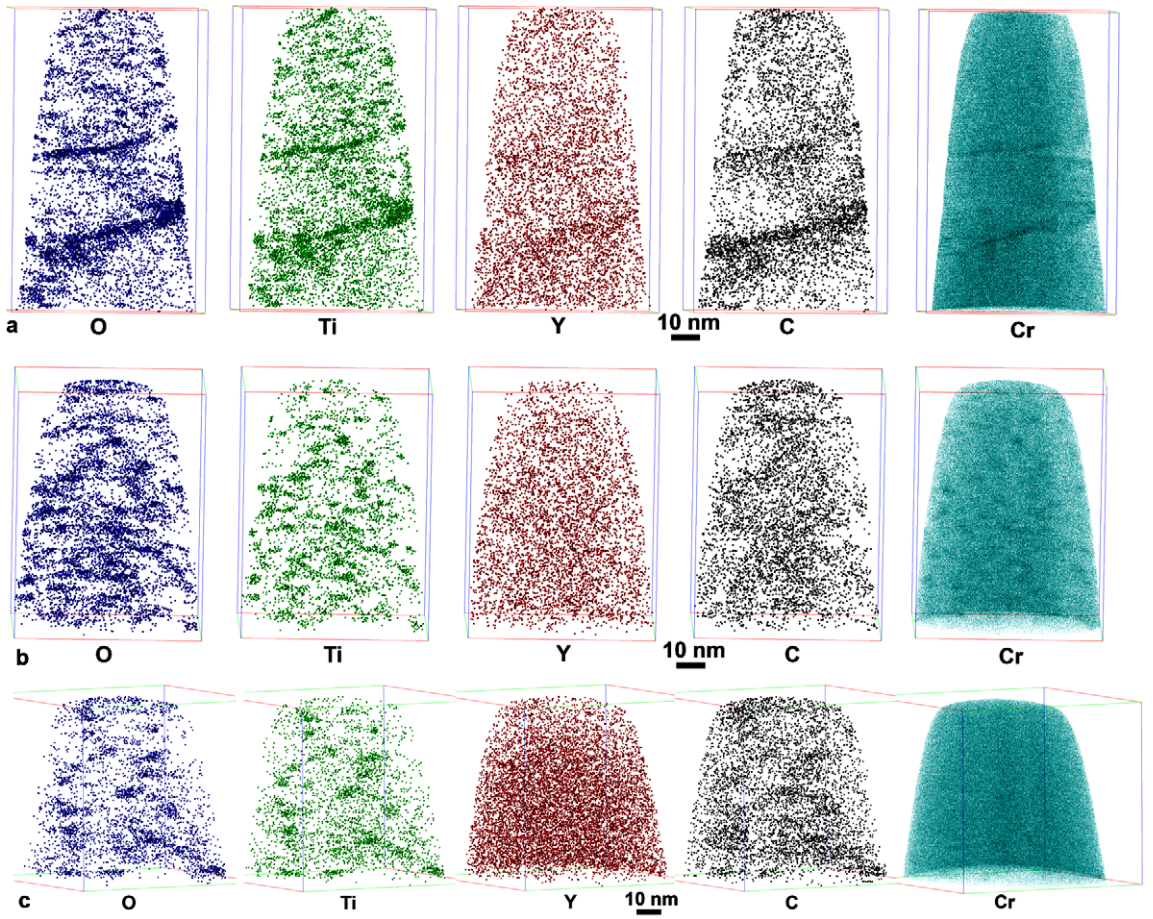

Fig. 4. Atom maps of the 14YWT alloys after extrusion, (a) SM alloy after 40 h milling, (b) CR alloy after 40 h milling and (c) SM alloy after 80 h milling.

number density of nanoclusters in the 14YWT alloy may be associated with the increased level of oxygen in the alloy and the presence of yttrium.

The average size and compositions of the nanoclusters in the 14YWT alloy as determined from the maximum separation envelope method are

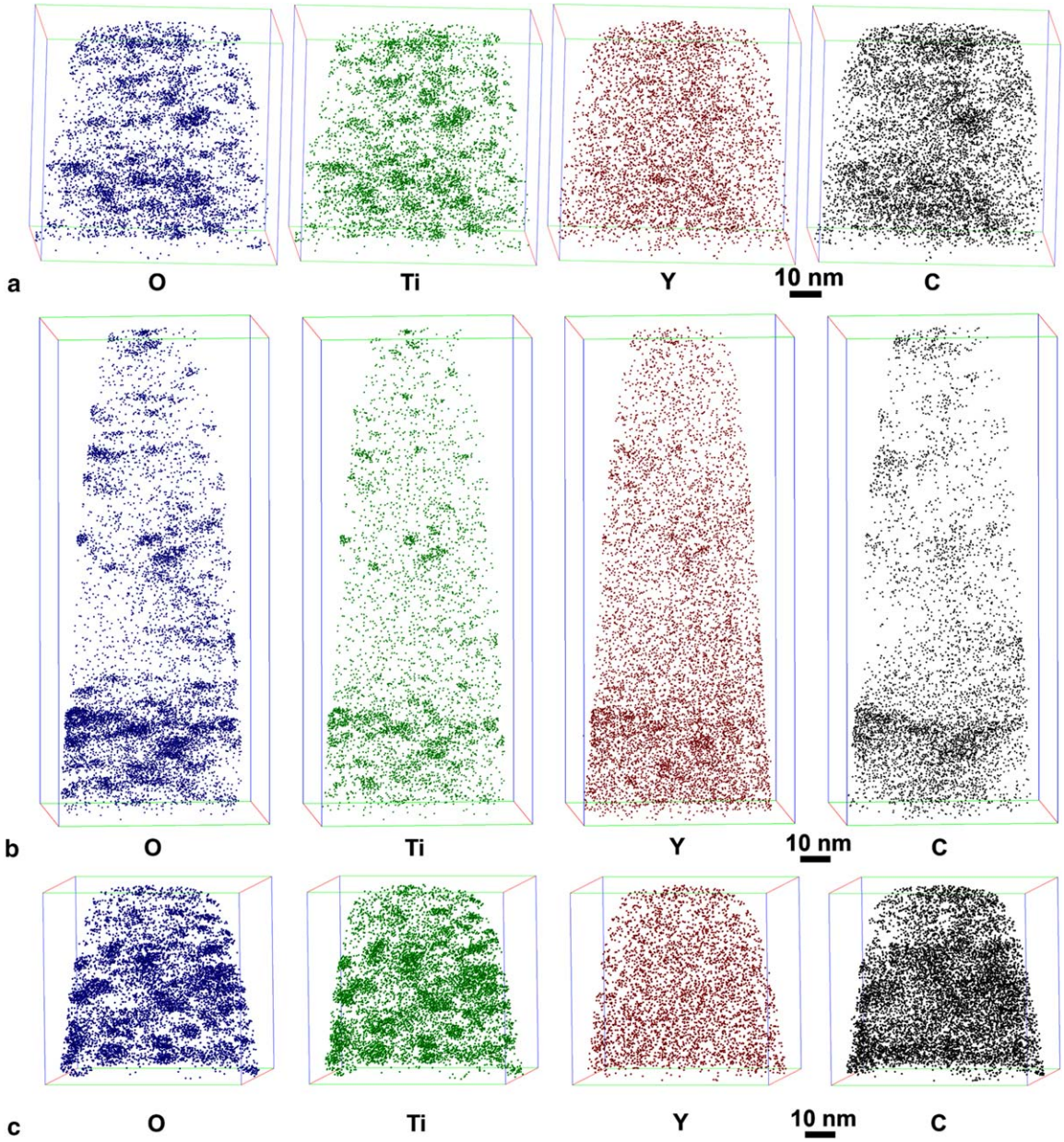

Fig. 5. Atom maps of the 14YWT alloys after thermal annealing for 1 h at 1000 °C, (a) SM alloy after 40 h milling, (b) CR alloy after 40 h milling and (c) SM alloy after 80 h milling.

summarized in Table 4. The diameter of these nanoclusters, ~2 nm, was significantly smaller than the original 17–31 nm Y_2O_3 powder. The metal-to-oxygen ratio was approximately 1:1 and there was substantially more titanium than yttrium in these nanoclusters indicating that the nanoclusters were consistent with TiO rather than the original Y_2O_3 powder. The yttrium distribution did not reveal any residual remnants with a Y_2O_3 stoichiometry. These results indicate that the Y_2O_3 powders were fully dissolved in the ferrite during the milling process. Some carbon and nitrogen were also detected in some of the nanoclusters. No significant difference was found between the 40 and 80 h milled conditions or between the different sources of powder. No significant difference was observed between the as-extruded and thermally aged conditions, indicating that the nanoclusters were remarkably resistant

Table 4
The size and composition of the titanium-, oxygen- and yttrium-enriched nanoclusters as estimated from the maximum separation method with $d_{max} = 0.6$ nm, $n_{min} = 25$ atoms and a grid spacing of 0.1 nm

Particle	14YWT-SM 40 h mill	14YWT-SM 80 h mill	14YWT-CR 40 h mill
As-extruded			
r_G, nm	1.0 ± 0.2	1.0 ± 0.2	0.9 ± 0.2
N_v, m^{-3}	4×10^{23}	2×10^{23}	2×10^{23}
Fe	5.5 ± 4.6	4.3 ± 3.7	3.6 ± 3.2
Cr	1.2 ± 1.1	0.8 ± 0.8	0.5 ± 0.5
W	0	0	0
Y	7.5 ± 4.3	5.1 ± 4.9	5.4 ± 4.5
Ti	42.2 ± 5.6	42.5 ± 4.1	43.8 ± 2.3
O	43.5 ± 5.3	47.2 ± 5.3	46.7 ± 3.8
1 h 1000 °C			
r_G, nm	0.9 ± 0.2	1.0 ± 0.2	1.0 ± 0.2
N_v, m^{-3}	1×10^{23}	1×10^{23}	7×10^{23}
Fe	3.4 ± 3.4	3.6 ± 1.8	4.5 ± 3.5
Cr	1.1 ± 1.1	0.8 ± 0.81	1.2 ± 1.2
W	0	0	0
Y	6.9 ± 5.8	4.3 ± 1.8	12.3 ± 8.8
Ti	43.9 ± 6.7	46.1 ± 1.7	37.6 ± 8.6
O	44.7 ± 4.0	45.1 ± 1.7	44.4 ± 4.6

Some carbon and nitrogen was detected in some of the nanoclusters.

to coarsening at elevated temperatures. These results are consistent with previous atom probe tomography investigations of 12YWT and MA957 alloys [13].

Ferritic alloys fabricated with traditional casting methods generally contain only a few parts per million of oxygen in the ferrite matrix with the remaining oxygen present in the alloy as coarse oxide inclusions. These MA/ODS ferritic alloys contain significantly higher concentrations of oxygen in the ferrite matrix. The presence of ultrafine titanium- and oxygen-enriched nanoclusters in the 14WT alloy reveals that the Y_2O_3 powder is not the only source of oxygen in these alloys. This oxygen is incorporated during the milling process from the dissolution of the Y_2O_3 powder particles, oxide and adsorbed oxygen on the surface of the metal powder, oxygen absorbed from the argon atmosphere during the milling process as well as any oxide inclusions present in the metal powder. Therefore, a much larger quantity of oxygen is available for reaction and precipitation than in traditional ferritic alloys. The non-uniform distribution of the nanoclusters indicates that the surface oxide locally increases the oxygen concentration and that the diffusion length scale is very small.

In order for the titanium-, yttrium-, and oxygen-enriched nanoclusters to nucleate and coarsen, these elements must diffuse through the ferrite lattice. However, the slow coarsening rate suggests that the diffusion rate of at least one of the elements is much slower than expected at high temperatures. Both yttrium and titanium atoms are significantly larger than iron atoms and therefore may be expected to be slow diffusers. However, the possibility of yttrium-vacancy or titanium-vacancy diffusion would significantly alter these diffusion rates. Oxygen would be expected to be a rapid diffuser in iron as it is an interstitial species. However, the ferrite matrix also contains significant levels of chromium, tungsten, titanium and yttrium as well as other residual elements. These elements can interact with the oxygen and form M–O complexes thereby retarding its diffusion rate. Some experimental support of this mechanism was observed as a substantial fraction of the titanium and oxygen detected from these nanoclusters was in the form of TiO^{++} molecular ions indicating a strong affinity between these elements.

The free energy of formation of the Y_2O_3 phase is higher than that of any of the titanium oxides [16], so that the most thermodynamically stable phase and the one that should form in this system is Y_2O_3 rather than the TiO phase that was observed. The low yttrium content in the nanoclusters would suggest that yttrium does not diffuse as fast as titanium. It is possible that the yttrium–oxygen interaction is sufficiently strong to form stable yttrium–oxygen complexes, thereby removing the bulk of the yttrium and some of the oxygen from participating in the nucleation and coarsening processes. This Y–O interaction mechanism would also support the coarsening observed in the 14WT alloy.

5. Conclusions

The fine scale precipitates and nanometer-scale clusters in mechanically alloyed, oxide-dispersion-strengthened (MA/ODS) ferritic alloys have been characterized by atom probe tomography. Atom probe tomography has revealed that these MA/ODS 14YWT ferritic alloys contain a high number density of ~2 nm diameter titanium-, yttrium- and oxygen-enriched nanoclusters in the as-extruded condition. These nanoclusters were found to be extremely resistant to coarsening at temperatures of at least 1000 °C. A lower number density of ~4–nm diameter titanium- and oxygen-enriched nanoclusters was observed in a yttrium-free 14WT

alloy. In this alloy, these nanoclusters coarsened to ~10 nm diameter after annealing at 1000 °C.

Acknowledgements

Research at the Oak Ridge National Laboratory SHaRE User Facility was sponsored by the Division of Materials Sciences and Engineering and the Office of Nuclear Energy, Science and Technology (I-NERI 2001-007-F), US Department of Energy, under contract DE-AC05-00OR22725 with UT-Battelle, LLC.

References

[1] G.D. Smith, J.J. deBarbadillo, in: J.J. deBarbadillo et al. (Eds.), Structural Applications of Mechanical Alloying, ASM International, Materials Park, OH, 1994, p. 117.
[2] S. Ukai, M. Harada, H. Okada, M. Inoue, S. Nomura, S. Shikakura, K. Asabe, T. Nishida, M. Fujiwara, J. Nucl. Mater. 204 (1993) 65.
[3] S. Ukai, M. Harada, H. Okada, M. Inoue, S. Nomura, S. Shikakura, T. Nishida, M. Fujiwara, J. Nucl. Mater. 204 (1993) 74.
[4] S. Ukai, T. Nishida, H. Okada, T. Okuda, M. Fujiwara, K. Asabe, J. Nucl. Sci. Tech. 34 (1997) 256.
[5] S. Ukai, T. Yoshitake, S. Mizuta, Y. Matsudaira, S. Hagi, T. Kobayashi, J. Nucl. Sci. Tech. 36 (1999) 710.
[6] I.-S. Kim, T. Okuda, C.-Y. Kang, J.-H. Sung, P.J. Maziasz, R.L. Klueh, K. Miyahara, Met. Mater. 6 (2000) 513.
[7] D.J. Larson, P.J. Maziasz, I.-S. Kim, K. Miyahara, Scripta Mater. 44 (2001) 359.
[8] I.-S. Kim, J.D. Hunn, N. Hashimoto, D.J. Larson, P.J. Maziasz, K. Miyahara, E.H. Lee, J. Nucl. Mater. 280 (2000) 264.
[9] E.A. Kenik, D.T. Hoelzer, P.J. Maziasz, M.K. Miller, Microsc. Microanal. 7 (2001) 550.
[10] M.K. Miller, E.A. Kenik, Microsc. Microanal. 8 (Suppl. 2) (2002) 1126-7CD.
[11] M.K. Miller, E.A. Kenik, K.F. Russell, L. Heatherly, D.T. Hoelzer, P.J. Maziasz, Mat. Sci. Eng. A 353 (2003) 140.
[12] M.K. Miller, D.T. Hoelzer, E.A. Kenik, K.F. Russell, Microsc. Microanal. 9 (Suppl. 2) (2003) 44.
[13] M.K. Miller, D.T. Hoelzer, E.A. Kenik, K.F. Russell, Intermetallics 13 (2005) 387.
[14] M.K. Miller, Atom Probe Tomography, Kluwer Academic/Plenum, New York, 2000.
[15] J.M. Hyde, C.A. English, in: G.E. Lucas, L. Snead, M.A. Kirk Jr., R.G. Elliman (Eds.), Proceedings of the MRS 2000 Fall Meeting, Symposium R: Microstructural Processes in Irradiated Materials, Boston, MA, November 27–30, 2000, vol. 650, Materials Research Society, Pittsburgh, PA, 2001, p. R6.6.1.
[16] D.R. Sigler, Oxid. Met. 32 (5–6) (1989) 337.